 https://doi.org/10.1051/e3sconf/202452003008

Proposing of a two-stage system known as the PV/T-ST system combining thermoelectric conversion technology for round-the-clock electrical output

Xin Wen[1,2], Jie Ji[1,2,*]

[1]Department of Thermal Science and Energy Engineering, University of Science and Technology of China, Hefei, Anhui, China
[2]Key Laboratory of Solar Thermal Conversion of Anhui Province, Hefei, Anhui, China

Abstract: In this study, a two-stage system known as the PV/T-ST system with a series photovoltaic/thermal (PV/T) module and a solar thermal (ST) collector combining thermoelectric conversion technology is proposed. In the daytime, the PV/T module generates power and captures low-temperature heat simultaneously. The ST module achieves secondary heating of water and secondary thermal-electric output by the thermoelectric generators (TEG). In the nighttime, the water heated by day continues to circulate, providing heat for TEG, thus achieving round-the-clock electrical output. Theoretical research reveals that the system's total electrical power reaches its maximum value at 11:57, measuring 97.43 W. The maximum heat gain amounts to 380.67 W. During the night, TEG operates continuously and experiences a gradual decline in electrical output, with an average electrical efficiency of 0.43%.

1 Introduction

Energy is a highly discussed topic in society as it profoundly impacts a nation's prosperity and people's lives [1]. To achieve the goal of "carbon neutrality" by 2060, it is urgent to build a clean, low-carbon, and secure energy system [2]. The PV/T system is able to simultaneously generate electricity and heat, significantly improving energy utilization efficiency compared to the photovoltaic (PV) system or the ST system [3]. Whereas, the PV/T system has a significant limitation in that it can only generate low-temperature heat, which cannot fully meet the heating needs of households or industries [4]. In comparison, the ST system achieves higher outlet temperatures and greater heat gain [5]. Besides, TEG generates electricity continuously, both during daylight hours and at night [6]. Therefore, this study emphasizes enhancing the electrical performance of solar systems and suggests a two-stage system known as the PV/T-ST system combining thermoelectric conversion technology to achieve round-the-clock power output.

2 System Overview

The two-stage system primarily consists of the PV/T module and the ST module, as shown in Fig. 1(a). When the system operates during the day, the system circulates the low-temperature water from the heat storage tank through the PV/T module. This process cools the module and dissipates excess heat produced by surplus solar energy which is not converted into electrical energy. Then, the water undergoes a secondary heat exchange process in the ST module before returning to the tank for storage. In the nighttime, the water continues to circulate in the system, releasing the stored heat to TEG, providing the conditions for TEG to output electricity at night. The characteristics of the water are outlined in Table 1.

Table 1. Performance Calculation of Water.

Property	Calculation Formula
Dynamic Viscosity (Pa·s)	$\mu_f = 1.788\times10^{-3}\exp\left(-1.704-\dfrac{1448.538}{T_f}+\dfrac{521926.58}{T_f^2}\right)$
Thermal Conductivity (W/(m·K))	$k_f = -0.000007843\times T_f^2+0.0062\times T_f-0.54$
Specific Heat Capacity (J/(kg·K))	$c_{p,f} = -0.0000463\times T_f^3+0.0552\times T_f^2-20.86\times T_f+6719.637$
Density (kg/m³)	$\rho_f = -0.0178\left\|T_f-277\right\|^{1.7}+1000\pm0.2\%$

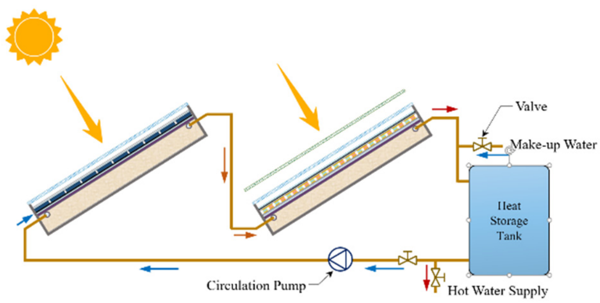

(a)

*Corresponding author's email: jijie@ustc.edu.cn

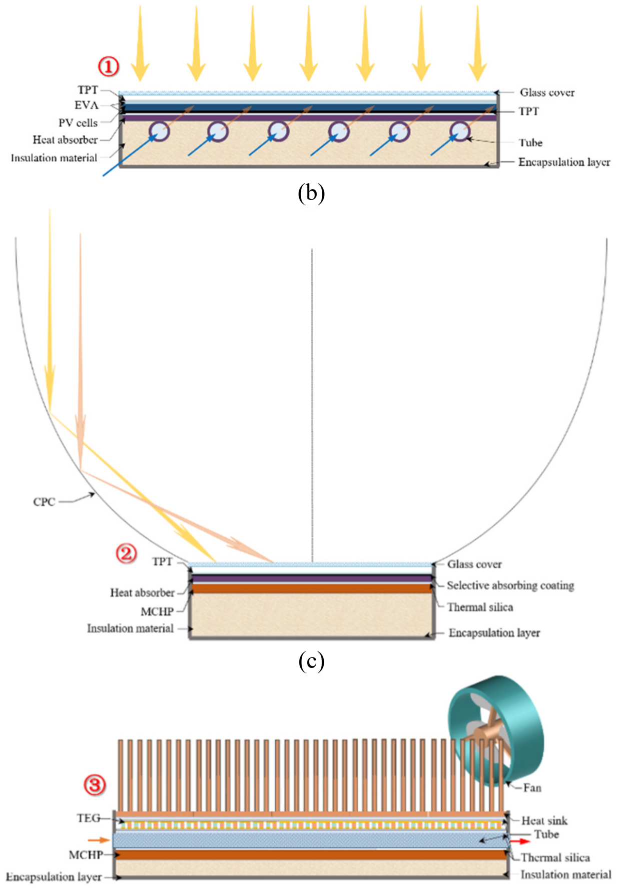

Fig. 1. System configuration.

Fig. 1(b) illustrates the specific layout of the PV/T module. The module has dimensions of 1214 mm×960 mm and consists of 35 PV cells, each measuring 156 mm×156 mm. The backside of the heat absorber features six tubes, each with a diameter of 11 mm, uniformly welded. PV captures solar radiation and transforms a portion of it into electricity, with the waste heat dissipated by the water. The ST module is segmented into the evaporator and condenser sections. The evaporator section has dimensions of 162 mm×960 mm and features a compound parabolic concentrator (CPC) with a fixed concentration ratio of 4 positioned above it, as depicted in Fig. 1(c). The heat absorber is coated with a selective absorption coating to enhance solar absorption and improve the thermal performance. The evaporator section of the microchannel heat pipe (MCHP) conveys the absorbed heat to the condenser section. As illustrated in Fig. 1(d), there is an attached insulation layer at the lower end of the condenser section, while the upper end is covered with a rectangular tube. The circulating water inside the tube carries away the heat from the condenser section. Some of the heat is obtained by the hot side of TEG connected to the tube, while the remaining heat is removed via the water for storage. Thermal silica is used to attach the heat sinks to the upper part of the cold side. A fan is employed to expedite the cooling process. At night, when PV is not operating, the heated water circulates and provides the heat for TEG, achieving round-the-clock output. The rectangular tube has a length of 162 mm and a cross-sectional area of 50 mm×15 mm.

Fig. 2 gives the TEG structure. The area of TEG is 50 mm×50 mm and its parameters are listed in Table 2 [7] .

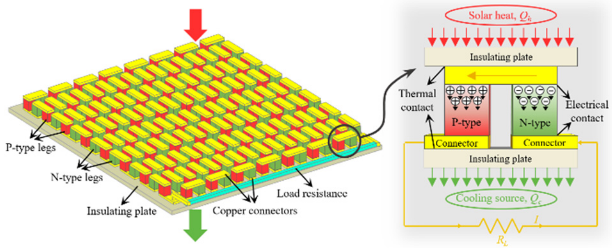

Fig. 2. Structure of TEG.

Table 2. Parameters of TEG.

Property	Value
TEG Figure of Merit (K⁻¹)	4.00×10⁻³
Seebeck Coefficient (V/K)	2.29×10⁻⁴
Electrical Resistivity (Ω·m)	7.23×10⁻⁶
Thermal Conductivity (W/(m·K))	1.82
Number	3
Area (m²)	50×50

3 Model Establishment

A quasi-steady-state mathematical model is developed for the PV/T-ST system, and the model is solved by MATLAB. The following assumptions are considered to facilitate the solution: the sky is treated as a blackbody; solar radiation is uniformly distributed on the system surface; all parallel tubes have the same thermal performance; the boundaries of framework are insulated.

3.1 The PV/T module

The heat transfer equation for the glass cover:

$$\delta_{g1}\rho_{g1}c_{p,g1}\frac{\partial T_{g1}}{\partial t}=h_a\left(T_a-T_{g1}\right)+h_{sky,g1}\left(T_{sky}-T_{g1}\right)+h_{g1,pv}\left(T_{pv}-T_{g1}\right)+G\alpha_{g1} \tag{1}$$

The heat transfer equation for PV:

$$\delta_{pv}\rho_{pv}c_{p,pv}\frac{\partial T_{pv}}{\partial t}=\delta_{pv}k_{pv}\left(\frac{\partial^2 T_{pv}}{\partial x^2}+\frac{\partial^2 T_{pv}}{\partial y^2}\right)+h_{ab1,pv}\left(T_{ab1}-T_{pv}\right)+h_{g1,pv}\left(T_{g1}-T_{pv}\right)+G\tau_{g1}\alpha_{pv}-\dot{E}_{pv} \tag{2}$$

The heat transfer equations for the heat absorber with and without connection to the tube:

$$\delta_{ab1}\rho_{ab1}c_{p,ab1}\frac{\partial T_{ab1}}{\partial t}=\delta_{ab1}k_{ab1}\left(\frac{\partial^2 T_{ab1}}{\partial x^2}+\frac{\partial^2 T_{ab1}}{\partial y^2}\right)++h_{ab1,pv}\left(T_{pv}-T_{ab1}\right)+\frac{T_{ch1}-T_{ab1}}{R_{ch1,ab1}\left(\mathrm{d}x\cdot\mathrm{d}y\right)}A_{ab1,i} \tag{3}$$

$$\delta_{ab1}\rho_{ab1}c_{p,ab1}\frac{\partial T_{ab1}}{\partial t}=\delta_{ab1}k_{ab1}\left(\frac{\partial^2 T_{ab1}}{\partial x^2}+\frac{\partial^2 T_{ab1}}{\partial y^2}\right)+h_{ab1,ba1}\left(T_{ba1}-T_{ab1}\right)+h_{ab1,pv}\left(T_{pv}-T_{ab1}\right) \tag{4}$$

The heat transfer equation for the tube:

$$\rho_{ch1}c_{p,ch1}A_{ch1}\frac{\partial T_{ch1}}{\partial t}=k_{ch1}A_{ch1}\left(\frac{\partial^2 T_{ch1}}{\partial y^2}\right)+\frac{A_{ch1,ab1}\left(T_{ab1}-T_{ch1}\right)}{\delta_{ch1,ab1}R_{ch1,ab1}}+\frac{A_{ch1,ba1}\left(T_{ba1}-T_{ch1}\right)}{\delta_{ch1,ba1}R_{ch1,ba1}}+P_{f1}h_{f1}\left(T_{f1}-T_{ch1}\right) \tag{5}$$

The heat transfer equation for the water:

$$\rho_{f1}c_{p,f1}A_{f1}\frac{\partial T_{f1}}{\partial t}=A_{f1}k_{f1}\frac{\partial^2 T_{f1}}{\partial y^2}+\dot{m}_{f1}c_{p,f1}\frac{\partial T_{f1}}{\partial y}+P_{f1}h_{f1}\left(T_{ch1}-T_{f1}\right) \tag{6}$$

The heat transfer equation for the encapsulation layer:

$$\delta_{ba1}\rho_{ba1}c_{p,ba1}\frac{\partial T_{ba1}}{\partial t}=h_a\left(T_a-T_{ba1}\right)+h_{ba1,ab1}\left(T_{ab1}-T_{ba1}\right) \tag{7}$$

3.2 The ST module

The heat transfer equation for the glass cover:

$$\delta_{g2}\rho_{g2}c_{p,g2}\frac{\partial T_{g2}}{\partial t}=h_{g2,a}\left(T_a-T_{g2}\right)+h_{sky,g2}\left(T_{sky}-T_{g2}\right)+h_{g2,ab2}\left(T_{ab2}-T_{g2}\right)+C_{cpc}G\alpha_{g2}\eta_{cpc} \tag{8}$$

The heat transfer equation for the heat absorber:

$$\delta_{ab2}\rho_{ab2}c_{p,ab2}\frac{\partial T_{ab2}}{\partial t}=\delta_{ab2}k_{ab2}\left(\frac{\partial^2 T_{ab2}}{\partial x^2}+\frac{\partial^2 T_{ab2}}{\partial y^2}\right)+h_{g2,ab2}(T_{g2}-T_{ab2})+\frac{\left(T_{ch2}-T_{ab2}\right)\cdot A_{ch2,i}}{R_{ab2,ch2}\cdot dx\cdot dy}+C_{cpc}G\tau_{g2}\alpha_{ab2}\eta_{cpc} \tag{9}$$

The heat transfer equation for MCHP:

$$m_{ev}c_{p,ev}\frac{\partial T_{ev}}{\partial t}=k_{hp}l_{hp}\left(T_{co}-T_{ev}\right)+h_{hp,ab2}A_{hp,ab2}\left(T_{ab2}-T_{ev}\right)+h_{hp,ba2}A_{hp,ba2}\left(T_{ba2}-T_{ev}\right) \tag{10}$$

$$m_{co}c_{p,co}\frac{\partial T_{co}}{\partial t}=k_{hp}l_{hp}\left(T_{ev}-T_{co}\right)+A_{ch2}h_{co,ch2}(T_{ch2}-T_{co}) \tag{11}$$

The heat transfer equation for the encapsulation layer:

$$\delta_{ba2}\rho_{ba2}c_{p,ba2}\frac{\partial T_{ba2}}{\partial t}=h_{ba2,a}\left(T_a-T_{ba2}\right)+h_{hp,ba2}\left(T_{ev}-T_{ba2}\right) \tag{12}$$

The heat transfer equations for the tube and water:

$$m_{ch2}c_{p,ch2}\frac{\partial T_{ch2}}{\partial t}=A_{ch2,s}k_{ch2}l_{f2}\frac{\partial^2 T_{ch2}}{\partial y^2}+A_{ch2}h_{te,ch2}\left(T_h-T_{ch2}\right)+A_{f2}h_{f2}\left(T_{f2}-T_{ch2}\right)+A_{ch2}h_{co,ch2}(T_{co}-T_{ch2}) \tag{13}$$

$$\rho_{f2}c_{p,f2}A_{f2}\frac{\partial T_{f2}}{\partial t}=A_{f2}k_{f2}\frac{\partial^2 T_{f2}}{\partial y^2}+\dot{m}_{f2}c_{p,f2}\frac{\partial T_{f2}}{\partial y}+P_{f2}h_{f2}\left(T_{ch2}-T_{f2}\right) \tag{14}$$

The heat transfer equation for TEG [8]:

$$\dot{Q}_h=se\cdot T_h I_{te}+\frac{T_h-T_c}{R_{te}}-\frac{I_{te}^2 r_{te}}{2}=A_{te}h_{te,ch2}(T_{ch2}-T_h) \tag{15}$$

$$\dot{Q}_c=se\cdot T_c I_{te}+\frac{T_h-T_c}{R_{te}}+\frac{I_{te}^2 r_{te}}{2}=A_{te}h_{te,sink}(T_c-T_a) \tag{16}$$

The heat transfer equation for the heat storage tank:

$$\rho_{f2}c_{p,f2}A_{ta}\frac{\partial T_{ta}}{\partial t}=A_{ta}k_{f2}\frac{\partial^2 T_{ta}}{\partial y^2}+n_{ch2}\dot{m}_{f2}c_{p,f2}\frac{\partial T_{ta}}{\partial y}+P_{ta}h_{ta}\left(T_a-T_{ta}\right) \tag{17}$$

3.3 Performance Assessment

The thermal performance is evaluated by the thermal output and thermal efficiency [9][10]:

$$\dot{Q}_{th}=n_{ch1}\dot{m}_{f1}c_{p,f1}\left(T_{f2}^1-T_{f1}^0\right) \tag{18}$$

$$\eta_{th}=\int_{t_1}^{t_2}\dot{Q}_{th}\mathrm{d}t\bigg/\int_{t_1}^{t_2}G\left(A_{g1}+A_{g2}\right)\mathrm{d}t \tag{19}$$

The electrical powers of PV and TEG [11, 12]:

$$\dot{E}_{pv}=G\tau_{g1}\alpha_{pv}\eta_{ref}A_{pv}\left[1-\beta_{ref}\left(T_{pv}-T_{ref}\right)\right] \tag{20}$$

$$\dot{E}_{te}=\sum_{1}^{n_{te}}\left(\dot{Q}_h-\dot{Q}_c\right)=\sum_{1}^{n_{te}}\left[se\cdot\left(T_h-T_c\right)I_{te}-I_{te}^2 r_{te}\right] \tag{21}$$

The electrical efficiencies of PV, TEG, and the whole system [13]:

$$\eta_{pv}=\int_{t_1}^{t_2}\dot{E}_{pv}\mathrm{d}t\bigg/\int_{t_1}^{t_2}GA_{g1}\mathrm{d}t \tag{22}$$

$$\eta_{te}=\int_{t_1}^{t_2}\dot{E}_{te}\mathrm{d}t\bigg/\int_{t_1}^{t_2}GA_{g2}\mathrm{d}t \tag{23}$$

$$\eta_{ele}=\eta_{pv}+\eta_{te} \tag{24}$$

The overall efficiency [14]:

$$\eta_{all}=\eta_{th}+\eta_{ele}/0.38 \tag{25}$$

4 Results and Discussion

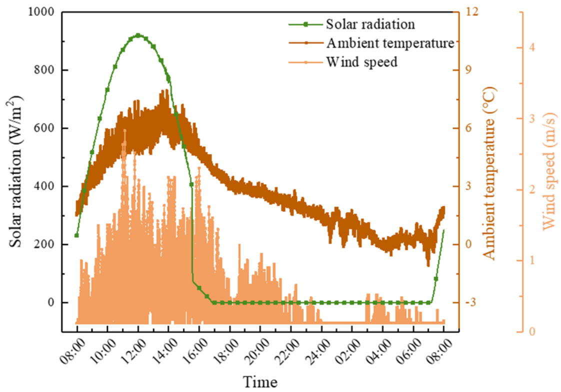

Fig. 3. Environmental Parameters in Hefei, Anhui Province.

Fig. 3 shows the measured environmental parameters of a certain day in Hefei, Anhui Province.

Fig. 4 presents the variation curve of instantaneous temperature. As the operation time progresses, the PV temperature, the temperature of the hot side of TEG, and the temperature of the cold side of TEG first rise and then decline. This can be easily understood as the temperature is influenced not only by the environmental temperature but also by the input energy and the water temperature. The solar radiation reaches its maximum value of 923.43 W/m^2 at 11:57 and decreases to 0 at 16:52. When the PV module receives more input energy, it maintains a higher temperature, with a maximum value of 36.73 ℃. As the solar radiation decreases, the PV temperature gradually decreases. However, due to the circulation of water, the water that absorbs heat during the day transfers heat to various components at night. As a result, the PV temperature does not reach the ambient temperature when the radiation becomes 0 but remains higher than the ambient temperature. At 15:32, the tank temperature is 31.08 ℃, surpassing the temperature of PV. This indicates that from this moment onwards, the outlet temperature of the tube is lower than the inlet temperature, indicating that heat transfer is occurring from the circulating water to PV. The continuous temperature difference between the hot and cold sides of TEG, influenced by heat transfer within the tube and the cooling effect of the heat sink, highlights the effective thermoelectric generation potential of TEG throughout the day. As the tank temperature gradually decreases overnight under cooling conditions on the cold side, the temperature difference across TEG reduces as well.

Fig. 5 depicts the fluctuation in the electrical power generated by the system throughout the day. The change in electrical power of PV follows a similar pattern to the solar radiation, because the PV output is mainly controlled by the input energy. The greater the energy density of the input, the higher the electrical output in that area. At 11:57, the PV power reaches its maximum value of 97.25 W and decreases to 0 at 16:52. The variation curve of electrical power of TEG is similar to that of the tank temperature. This is because, with a constant fan speed of 2 m/s, the generation capacity of TEG mainly depends on the temperature of the water passing beneath it, which is determined by the tank temperature. At 15:32, a significant drop in solar radiation leads to a notable decrease in the temperature of the hot side of TEG, resulting in noticeable fluctuations in TEG power. Given the significant contribution of PV in comparison to TEG, the total electrical power displays a trend of increasing followed by decreasing, mirroring the fluctuations in the electrical power of PV. Fig. 6 presents the variation curves of PV, TEG, and total electrical efficiencies by day. It is evident that with the exception of the electrical efficiency of TEG, both the PV efficiency and the total electrical efficiency exhibit a decrease followed by an increase. This pattern contrasts with their power variations because efficiency is influenced by both output and input levels. When the PV output is high, the system receives a large input energy, and the rate of increase in input energy exceeds the rate of increase in power, resulting in opposite trends in efficiency and power. But for TEG, the direct factor affecting its output is the temperature difference. The rate of change in temperature difference exceeds the rate of change in the heat it receives, causing the TEG efficiency to follow the same trend as its power. The minimum total electrical efficiency occurs at 11:59, with a value of 9.72%.

Fig. 7 displays the thermal performance during the day. Following 15:32, as the water temperature at the outlet is lower than that at the inlet, Fig. 7 only shows the change of heat gain from 8:00 to 15:32. The instantaneous heat gain also follows a pattern of first increasing and then decreasing, with a maximum value of 380.67W owing to the impact of cooling. The thermal efficiency ranges from 0% to 25%, where the low thermal efficiency is attributed to the calculation considering the sum of the areas of the two modules in the denominator, and the cooling of the heat sink weakens the heat collection. The overall efficiency is calculated by taking into account the varying energy grades of electrical energy and thermal energy. In the daytime, the overall efficiency exhibits a pattern of increasing followed by decreasing, as a result of the combined impact of electrical efficiency and thermal efficiency, averaging at 44.35%.

Fig. 8 demonstrates the variation of the electrical performance during the night. Obviously, the electrical output of TEG at night decreases continuously. This is because the circulating water transfers heat to the system, and with the passage of time, the circulating water holds less heat at a lower temperature, causing a decrease in the temperature difference across TEG. Fig. 8 also illustrates a decrease in the electrical efficiency of TEG during the night, averaging at 0.43%.

The circulating water effectively slows down the rate of decrease in electrical power and even provides certain thermal conditions for TEG in the absence of solar radiation, ensuring continuous output throughout the day. Although the current power generation capacity of TEG is limited, it is believed that with technological advancements, the TEG performance will significantly improve, and the application of the nighttime output of TEG in solar systems will become increasingly necessary.

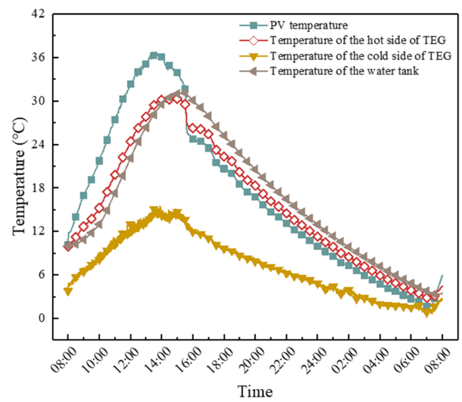

Fig. 4. Variation of System Temperature.

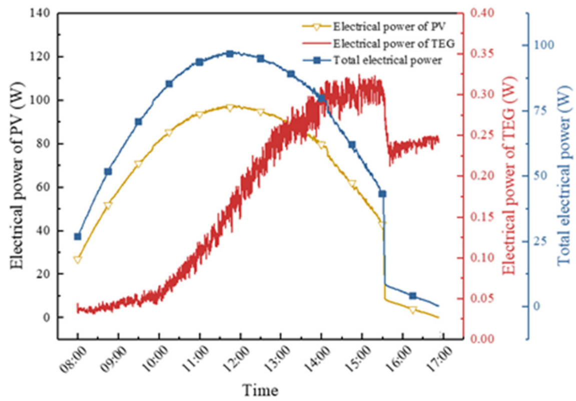

Fig. 5. Variation of Electrical Power by Day.

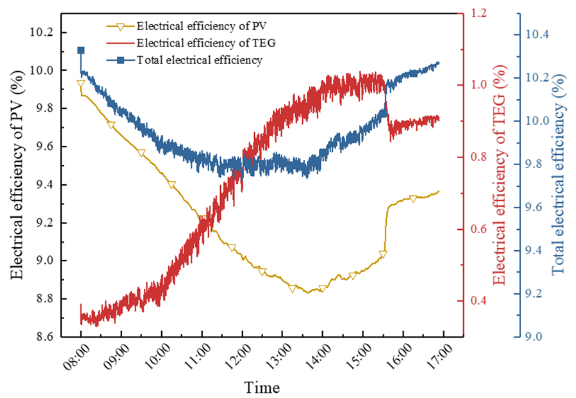

Fig. 6. Variation of Electrical Efficiency by Day.

5 Conclusions

A two-stage PV/T-ST system combining thermoelectric conversion technology is proposed. The PV/T module is responsible for generating both electricity and heat, while the ST module facilitates the production of secondary heating water and secondary thermoelectric output during daytime operation. At night, the heated water is used to provide heat for power generation of TEG, achieving round-the-clock output. In the daytime, the total electrical power reaches its maximum value of 97.43 W at 11:57. Due to the weakening of the heat collection by heat sinks, the thermal efficiency varies between 0% and 25%, and the largest heat gain is 380.67 W. During nighttime operation, the circulating water gradually transfers less heat to the system as it carries heat at a lower temperature with prolonged operation time. Consequently, the TEG output decreases, with an average efficiency of 0.43%. Now, the power generation capacity of TEG is limited, so how to enhance TEG performance is a major consideration for future research.

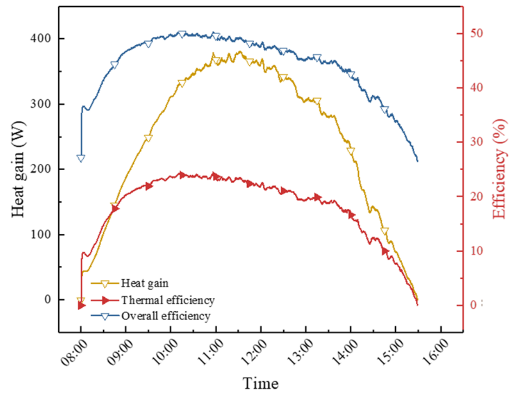

Fig. 7. Variation of Thermal Performance at Day.

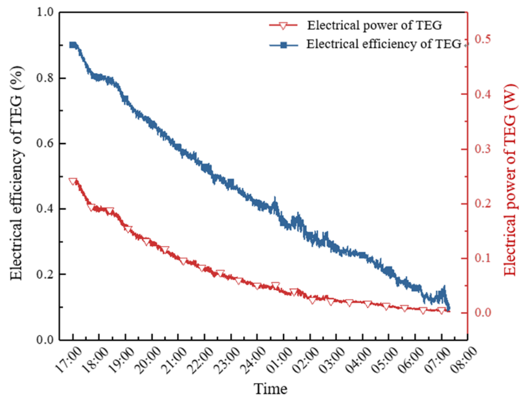

Fig. 8. Variation of Electrical Performance at Night.

Acknowledgements

This project receives funding from the National Natural Science Foundation of China (No. 52238004) and Anhui Provincial Major Science and Technology Project (202203a07020021).

References

1. M.M. Uddin, J. Ji, C. Wang, C. Zhang. Building energy conservation potentials of semi-transparent CdTe integrated photovoltaic window systems in Bangladesh context. Renewable Energy. 207 (2023) 512-30.
2. X. Tang, G. Li, X. Zhao, K. Shi, L. Lao. Simulation analysis and experimental validation of enhanced photovoltaic thermal module by harnessing heat. Applied Energy. 309 (2022).
3. X. Kong, L. Zhang, H. Li, Y. Wang, M. Fan. Experimental thermal and electrical performance analysis of a concentrating photovoltaic/thermal system integrated with phase change material. Solar Energy Materials and Solar Cells. 234 (2022).
4. T. Ma, M. Li, A. Kazemian. Photovoltaic thermal module and solar thermal collector connected in series to produce electricity and high-grade heat simultaneously. Applied Energy. 261 (2020).
5. M. Li, D. Zhong, T. Ma, A. Kazemian, W. Gu. Photovoltaic thermal module and solar thermal collector connected in series: Energy and exergy analysis. Energy Conversion and Management. 206 (2020).
6. B. Zhao, M. Hu, X. Ao, Q. Xuan, Z. Song, G. Pei. Is it possible for a photovoltaic-thermoelectric device to generate electricity at night? Solar Energy Materials and Solar Cells. 228 (2021).
7. Y.-Y. Wu, S.-Y. Wu, L. Xiao. Performance analysis of photovoltaic–thermoelectric hybrid system with and without glass cover. Energy Conversion and Management. 93 (2015) 151-9.
8. M. Du, G.H. Tang, T.M. Wang. Exergy analysis of a hybrid PV/T system based on plasmonic nanofluids and silica aerogel glazing. Solar Energy. 183 (2019) 501-11.
9. X. Zhang, X. Zhao, S. Smith, J. Xu, X. Yu. Review of R&D progress and practical application of the solar photovoltaic/thermal (PV/T) technologies. Renewable and Sustainable Energy Reviews. 16 (2012) 599-617.
10. N. Zheng, H. Zhang, L. Duan, Q. Wang, A. Bischi, U. Desideri. Techno-economic analysis of a novel solar-driven PEMEC-SOFC-based multi-generation system coupled parabolic trough photovoltaic thermal collector and thermal energy storage. Applied Energy. 331 (2023).
11. A. Hassan, S. Abbas, S. Yousuf, F. Abbas, N.M. Amin, S. Ali, et al. An experimental and numerical study on the impact of various parameters in improving the heat transfer performance characteristics of a water based photovoltaic thermal system. Renewable Energy. 202 (2023) 499-512.
12. Z. Song, J. Ji, J. Cai, Z. Li, Y. Gao. Performance prediction on a novel solar assisted heat pump with hybrid Fresnel PV plus TEG evaporator. Energy Conversion and Management. 210 (2020).
13. H. Alghamdi, C. Maduabuchi, D.S. Mbachu, A. Albaker, I. Alatawi, T.R. Alsenani, et al. Machine learning model for transient exergy performance of a phase change material integrated-concentrated solar thermoelectric generator. Applied Thermal Engineering. 228 (2023).
14. Z. Li, J. Ji, W. Yuan, Z. Song, X. Ren, M.M. Uddin, et al. Experimental and numerical investigations on the performance of a G-PV/T system comparing with A-PV/T system. Energy. 194 (2020).